GSI

GSI-Preprint-96-39
August 1996



# DETAILED INVESTIGATIONS OF TWO-CENTER COLLISION DYNAMICS

R.E. OLSEN, C.R. FEELER, C.J. WOOD, C.L. COCKE, R. DÖRNER, V. MERGEL,
H. SCHMIDT-BÖCKING, R. MOSHAMMER, J. ULLRICH



(Submitted to Nucl. Instr. Meth.)

Gesellschaft für Schwerionenforschung mbH
Planckstraße1 • D-64291 Darmstadt • Germany
Postfach 110552 • D-64220 Darmstadt • Germany

# Detailed Investigations of Two-Center Collision Dynamics

R. E. Olson[1], C. R. Feeler[1], C. J. Wood[1], C. L. Cocke[2], R. Dörner[3], V. Mergel[3], H. Schmidt-Böcking[3], R. Moshammer[4] and J. Ullrich[4]

[1]Department of Physics, University of Missouri, Rolla, MO 65401, U.S.A.

[2]J. R. Macdonald Laboratory, Kansas State University, Manhattan, KS 66506, U.S.A.

[3]Institut für Kernphysik, University of Frankfurt, D-60486 Frankfurt/Main, Germany

[4]Gesellschaft für Schwerionenforschung, D-64220 Darmstadt, Germany

**Abstract**

The combination of recoil ion and ionized electron momentum spectroscopy provides an unparalleled method to investigate the details of ion-atom collision dynamics. In order to predict scattering behavior and collaborate with experimental projects, the classical trajectory 3- and n-body Monte Carlo method has been modified to yield complete momenta information for ionized electron spectra in the collision plane defined by the incident projectile and outgoing projectile or recoil ion. To illuminate the richness of these spectra, calculations of 300 and 500 keV p and $p^-$ single ionization collisions with He are presented for low q/v perturbation strengths. For strong q/v collisions, the 100, 300 and 500 keV/u $Ne^{10+}$ on He systems are illustrated. Strong asymmetry of the slow and saddle point electrons are predicted for antiproton and highly-charged $Ne^{10+}$ projectiles. Furthermore, The electron capture to the continuum spectra for $Ne^{10+}$ are observed to have not only the expected asymmetry in the longitudinal direction, but also a strong asymmetry in the collision plane.

**FIAC '96, Nucl. Instru. Methods B**

## Introduction

The experimental application of recoil ion momentum spectroscopy has rapidly matured over just a few years. Originally, recoil ions were used as a source of slow, multiply-charged ions which were then employed in subsequent collision measurements. In the late 1980's, Ullrich and Schmidt-Böcking were the first to actually measure the momenta of recoil ions and deduce collision mechanisms from transverse momentum distributions (see Ref. [1] for a review). These early measurements were severely limited by the thermal motion of the target atoms which markedly restricted the precision of the observations.

The development of "cold" targets and position sensitive detection have removed many of the impediments of the method. As an example, Dörner *et al.* [2] displayed the interplay of three-body collision dynamics for $H^+$ + He single ionization collisions. The Kansas State group lead by Cocke was able to clearly observe the mass transfer of the electron [3] in multiple electron capture collisions of $F^{9+}$ + Ne. These measurements were followed by the direct observation of the signatures of the electron-electron and electron-nuclear interactions in $He^+$ + He projectile ionization [4]. Very recently, Moshammer *et al.* have performed the first complete momentum determination of the products in single ionization collisions [5] and have clearly observed the importance of the electron-electron interaction in multiple ionization collisions [6]. The French group at Caen [7] has made high precision state-selective electron capture measurements using recoil ion momentum spectroscopy for low energy collisions involving $Ne^{10+}$ and $Ar^{18+}$ .

Presently, new experiments by Mergel [8] illuminate the e-e Thomas mechanism for transfer ionization in $H^+$ + He collisions, while Kravis *et al.* [9] investigated slow electron production in low energy collisions involving multiply-charged ions. Furthering the

development of the field is the investigation by Dörner *et al.* [10] who observed collision plane information for slow electron production in 10 and 15 keV $H^+$ + He collisions.

Unfortunately, theoretical methods that describe the complete final state momentum information for single and multiple electron removal have not made the spectacular advances as those of the experimentalists. The major impediment is the lack of a quantal theory that can provide coincidence information of the products for even a 3-body single ionization reaction, let alone multiple ionization processes. Basis set expansion methods, while providing excellent accuracy for 2-body interactions such as excitation and electron capture, are unable to provide momentum information for ionized electrons since the pseudostates used to represent the ionization channel do not have sufficient angular information.

In order to fill the gap and provide interpretation and predictions of scattering dynamics, we were lead to develop the n-body classical trajectory Monte Carlo method [11]. In the CTMC method, the collision is evolved using classical mechanics, while the initial conditions contain necessary quantal information. A merit of the method is that all the electron-nuclear and nuclear-nuclear interactions are included so that it is possible to do a complete determination of the momenta of the product states of a collision. In order to maintain parity with the experimental progress noted above, incremental extensions have been made to the CTMC method so that now model potentials based on Hartree-Fock calculations can be used to describe the electron-nuclear interactions [12], electrons on both target and projectile centers can be incorporated [4], dynamical screening of the nuclei during the collision [13], and direct inclusion of the e-e interaction in the post collision regime [6].

The motivation for the work reported here is to predict signatures of single ionization dynamics using coincidence procedures that are now within the reach of the sophisticated recoil ion momentum spectroscopy experiments. The range of projectile charge state over

collision speed q/v is varied so that both weak perturbation strengths and strongly perturbed systems are investigated. Further, antiproton collisions are studied to provide insight into experiments that are now taking place at CERN. As in the experiments, we have concentrated on the He target. For low q/v collisions, p and $p^-$ at 300 and 500 keV are illustrated; the 100 keV cases have already been published by Wood *et al.* [14] and are the subject of a detailed study in a forth coming publication [15]. For strongly coupled systems $Ne^{10+}$ at 100, 300 and 500 keV/u is illustrated since it nicely displays the commonly referred to soft, saddle point, and electron capture to the continuum electron emission signatures. Collision plane information is given, along with aspects of the impact parameter dependence of the individual processes by restricting the range of transverse momenta of the recoil ion.

## Method

The classical trajectory Monte Carlo method has been previously described in detail [11,16]. Important for the application to recoil ion spectroscopy is the initialization of the target atom so that its total center-of-mass momentum is zero. If only the momentum of the target nucleus is set equal to zero as is usually done, the motion of its electrons will induce a non-zero threshold energy for the recoil ion which is the same order as that caused by all but the hardest collision.

In the calculations presented here, we have used a modified Wigner distribution [17] for the He atom's electronic representation. The method is the same as that used previously for the hydrogen atom [18] and greatly improves the classical radial distribution. For the He atom we have employed ten binding energies between 2.70 and 0.36 a.u. These binding energies are then weighted so that the resulting classical microcanonical radial distribution

provides a fit to the exact quantal result. For He, this procedure results in an excellent fit of the microcanonical results to the quantal radial probability to 5 $a_o$ and fortuitously, a much better comparison with the quantal momentum probability than previously achieved.

The advantage of employing the Wigner distribution is that the microcanonical distributions for the radial and momentum probabilities are in excellent accord with quantum mechanical calculations. In turn, this results in a better description of the soft, large impact parameter collisions. However, the finite value for the binding energy is lost by using the Wigner distribution. This manifests itself in the calculated longitudinal momentum distributions not having a sharp cutoff at $-U/v_p$ for the projectile momentum change, and at $-U/v_p - v_p/2$ for the recoil ion, where the binding energy U is 0.9033 a.u. for He and $v_p$ is the projectile speed.

**Results and Discussion**

To illustrate the weak collision regime, calculational results are presented for 300 and 500 keV p and $p^-$ single ionization collisions with He. Perturbation strengths q/v for these collisions are 0.289 and 0.224, respectively. Furthermore, for such relatively fast collisions the electron capture channel is negligible so that the electrons are expected to be primarily target centered.

Displayed in Fig. 1 are calculated spectra for the longitudinal momenta of the ionized electron and recoil ion, and the change in momenta of the projectile. In all our calculations, the initial direction of the projectile is along the +z axis. For both energies, the proton and antiproton projectile spectra are quite similar, with the only significant difference being that the magnitude of the proton cases is slightly larger than for the antiproton cases, consistent

with the experimental absolute cross sections [19]. However, significant differences are predicted for the electron and recoil ion spectra which are found to have reversed positions and widths. For fast, perturbative collisions the ionized electrons tend to be ejected close to 90°, i.e. $p_z$ = 0.0 a.u., however, in the proton cases the electrons do have a preference for forward angle ejection due to the attractive interaction between proton and electron. For antiprotons, the opposite is observed. Interestingly, the widths of the spectral peaks indicate that the electrons are more concentrated for antiproton than for proton collisions, reflecting the longer post collision interaction for the protons.

As yet, there are no experimental antiproton spectra with which to compare the trends predicted by the calculations. Data do exist for the ejected electron differential cross sections for the proton cases (see Ref. [20] for a review). These cross sections which are doubly differential in scattering angle and energy can easily be transformed into longitudinal momentum spectra; the absolute cross sections of the early work [20] were normalized to be consistent with the more recent analysis of Ref. [21]. As expected the CTMC results underestimate the true ionization cross sections at high energies. However, the general trends are consistent with experiment. This is further borne out by favorable comparisons of the calculated and experimental transverse momenta spectra of the electrons and recoils at 500 keV [22].

It is interesting to probe the collision dynamics further and investigate more highly differential spectra. Presented in Fig. 2 are calculated event spectra of the proton and antiproton systems for electron momenta which are in the plane defined by the initial projectile direction +z and final recoil ion transverse direction +x. The circles depict the binary encounter ring. Further analysis shows the electron spectra for proton impact to be cylindrically symmetric around $p_x$ = 0.0 a.u. indicating that the dominant interaction of the

projectile is with the electron, not the recoil.

However, the antiproton cases are decidedly asymmetric along the x axis. This is the result of the coulomb interaction of the electron with the negative charge of the antiproton. At the distance of closest approach, the antiproton attracts the $He^+$ recoil towards it, but repels the electron in the opposite direction. Since there is no strong post collision interaction that attracts the electrons to the +z direction as in the proton case, the electrons tend to be preferentially found at negative $p_x$ values. Binary encounter electrons are easily observed for the antiproton cases, unlike in the proton system where forward ejected electrons make observation difficult.

To explore the strong coupling regime, we have chosen the 100, 300 and 500 keV/u $Ne^{10+}$ + He systems; the respective perturbation strengths q/v are 5.00, 2.89 and 2.24. The rationale for these choices is that at 100 keV/u the theoretical predictions extend the work already presented by Kravis *et al.* [9], while at the highest energy the results possess almost the same q/v as the 3.6 MeV/u $Se^{28+}$ studies of Moshammer *et al.* [5]. Furthermore, one would expect the $Ne^{10+}$ systems to possess rich spectra since at 100 keV/u electron capture dominates, while at 500 keV/u impact ionization is the preferred electron removal process.

The calculated longitudinal momentum spectra for the electron, recoil ion and projectile are displayed in Fig. 3. It is apparent that all 3-bodies share in the final state momentum balance, unlike at higher energies where the change in momentum of the projectile is almost a delta function which results in a strong 2-body interaction between recoil and electron [5]. The width of the change in momentum of the projectile is decreasing with increasing energy, but it still is significant even at 500 keV/u. It is surprising that the high momentum component of the forward ejected electrons decreases with increasing energy between 300 and 500 keV/u. This is probably due to the decreasing importance of the

electron capture channel with the resulting decrease of electron capture to the continuum component in the electron spectra.

If all the electron events are now projected onto the projectile - recoil plane, additional features of the ionization process are illuminated, Fig. 4. There is a pronounced trend for the intermediate and fast electrons to be ejected with negative values of $p_x$, or in the direction opposite to that of the recoil ion. Analysis of the azimuthal angle between the projectile and recoil always produces values near 180°. Hence, the asymmetry implies that the intermediate to fast electrons are experiencing the strong attractive coulomb interaction of the projectile and are tracking with it. In contrast there is a tendency for the slow electrons to be emitted with the recoil rather than the projectile. At first we attributed this behavior to large impact parameter collisions mediated by the polarization interaction. However, detailed analysis of these trajectories did not confirm negative deflection angles. Both the recoil and electron balance the transverse momentum of the projectile for these collisions. At 100 keV/u there is a considerable fraction of the collisions that gives rise to intermediate speed two-center electrons which many would term saddle point electrons. Moreover, even at 100 keV/u there is no pronounced electron capture to the continuum peak in the collision plane information presented at this level. Note, we have also plotted the events in the collision plane determined by the incident and final projectile momenta. The comparison is complimentary to that given and does not offer the resolution advantage of the projectile - recoil frame to experimental observations.

It is also of interest to plot the results in the plane perpendicular to the projectile - recoil plane, Fig. 5. Here, all electrons have been projected onto the y-z plane. These spectra are narrower than those of Fig. 4, implying a preference for the ionized electrons to be emitted in a "oyster shell" shape with its opening in the plane defined by the projectile and

recoil ion.

If the event spectra of Fig. 4 are presented differential in only those electrons which are in the collision plane, $|p_y^d| \leq 0.05$ a.u., the spectral features change considerably, Fig. 6. At all energies a peak due to the slow electrons is present. However, most of the intermediate speed electrons are not present, implying they are emitted out-of-plane of the heavy nuclei. At 100 keV/u the electron capture to the continuum (ECC) peak is clearly present and is asymmetrically peaked as expected on the low side of $p_z = v_p$. However, we also note a tendency for the ECC peak to appear at negative values of $p_x$ , implying the collisions giving rise to ECC are violent enough to cause a noticeable deflection of the projectile by the recoil ion, which would not be the case if the projectile was dominated by the projectile - electron scattering.

We can further investigate the collision plane dependence of all outgoing products by also displaying the recoil ion and projectile momenta in coincidence with the electrons that are emitting in the projectile-recoil plane. As an example we have chosen the 100 keV/u case, Fig. 7. Here it can be easily observed that the recoil and projectile are preferentially scattered opposite to one another, $+p_x$ for the recoil and $-p_x$ for the projectile. As expected the projectile is at negative values of $p_z$ being ionization is an exoergic reaction. Moreover, it appears the electron and projectile must coherently combine their transverse momenta in order to balance that of the recoil ion.

As accomplished experimentally and theoretically by Dörner *et al.* [10], it is possible to further dissect the collision process by presenting collision plane information in coincidence with the magnitude of the transverse momentum of the recoil ion. By such a selection, low recoil momenta probe the large impact parameter collisions while the large recoil momenta relate to the more violent close collisions. In Fig. 8 are displayed the 100 keV/u collision

plane results of Fig. 6 for low, intermediate and large values of transverse recoil momenta. As the violence of the collision increases with the transverse recoil momenta, we observe a distinct trend to proceed from the production of slow electrons to a preference to mainly produce the ECC peak. Asymmetries in both the $p_x$ and $p_z$ components are again observed.

## Concluding Remarks

The field of momentum spectroscopy has matured rapidly in just the last several years. This progress has been lead by major advances in experimental techniques developed at the University of Frankfurt, GSI-Darmstadt and Kansas State University. In turn the theoretical advances have been mainly prompted by the close collaboration with the experimentalists. This synergism continues to be advantageous to both theory and experiment where each of which can make predictions and observations that can be tested by the other. It is the purpose of this progress report to make predictions that will be tested by experimental observation in the very near future. It appears that collision plane coincidence studies of multiply-charged ion collisions involving projectiles such as $C^{6+}$ or $Ne^{10+}$ at energies around 100 to 200 keV/u will yield considerable insight into a wide variety of basic collision processes.

## Acknowledgments

The authors would like to thank the Office of Fusion Research of the U.S. Department of Energy, the Bundesministerium für Bildung und Forschung, the Deutsche Forshungsgemeinshaft, and the National Science Foundation Int 9112815 for their support.

## References


[1] C. L. Cocke and R. E. Olson, *Phys. Rep.* **205** (1991) 153.

[2] R. Dörner, J. Ullrich, H. Schmidt-Böcking and R. E. Olson, *Phys. Rev. Lett.* **63** (1989) 147.

[3] V. Frohne, S. Cheng, R. Ali, M. Raphaelian, C. L. Cocke and R. E. Olson, *Phys. Rev. Lett.* **71** (1993) 696.

[4] R. Dörner *et al. Phys. Rev. Lett.* **72** (1994) 3166.

[5] R. Moshammer *et al. Phys. Rev. Lett.* **73** (1994) 3371.

[6] R. Moshammer *et al. Phys. Rev. Lett.* **77** (1996) in press.

[7] A. Cassimi, S. Duponchel, X. Flechard, P. Jardin, P. Sortais, D. Hennecart and R. E. Olson, *Phys. Rev. Lett.* **76** (1996) 3679.

[8] V. Mergel, Ph.D. Thesis, University of Frankfurt, 1996.

[9] S. D. Kravis *et al. Phys. Rev. A* **54** (1996) in press.

[10] R. Dörner, H. Khemliche, M. H. C. L. Cocke, J. A. Gary, R. E. Olson, V. Mergel, J. Ullrich and H. Schmidt-Böcking, *Phys. Rev. Lett.* **77** (1996) submitted.

[11] R. E. Olson, J. Ullrich and H. Schmidt-Böcking, *Phys. Rev. A* **39** (1989) 5572.

[12] D. R. Schultz, C. O. Reinhold and R. E. Olson, *Phys. Rev. A* **40** (1989) 4947.

[13] V. J. Montemayor and G. Schiwietz, *Phys. Rev. A* **40** (1989) 6223.

[14] C. J. Wood and R. E. Olson, *J. Phys. B* **29** (1996) L257.

[15] C. J. Wood, J. A. Gary, C. R. Feeler and R. E. Olson, *Phys. Rev. A* submitted.

[16] R. E. Olson and A. Salop, *Phys. Rev. A* **16** (1977) 531.

[17] D. Eichenaur, N. Grün and W. Scheid, *J. Phys. B* **14** (1981) 3929.

[18] D. J. W. Hardie and R. E. Olson, *J. Phys. B* **16** (1983) 1983.

[19] P. Hvelplund, H. Knudsen, U. Millelsen, E. Morenzoni, S. P. Møller, E. Uggerhøj and T. Worm, *J. Phys. B* **27** (1994) 925.

[20] M. E. Rudd, L. H. Toburen and N. Stolterfoht, *At. Data Nucl. Tables* **18** (1976) 413.

[21] R. D. DuBois and S. T. Manson, *Phys. Rev. A* **35** (1987) 2007.

[22] R. Dörner, V. Mergel, L. Zhaoyuan, J. Ullrich, L. Spielberger, R. E. Olson and H. Schmidt-Böcking, *J. Phys. B* **28** (1995) 435.

**Figure captions**

1. Longitudinal momentum spectra for the recoil ion, ejected electron, and change in momentum of the projectile for proton and antiproton collisions with He at 300 and 500 keV. The solid points are electron values obtained from an analysis of doubly differential spectra given in Ref. [20]. The absolute values of the data of [20] were renormalized to the more recent results [21].

2. Ionized electron event spectra for 300 and 500 keV proton and antiproton collisions in the collision plane defined by the incident projectile (+z direction) and the transverse momentum of the recoil ion (+x direction). The ovals represent the binary encounter ring.

3. Longitudinal momentum distributions for 100, 300 and 500 keV/u $Ne^{10+}$ + He single ionization collisions.

4. Ionized electron spectra for 100, 300 and 500 keV/u $Ne^{10+}$ projected onto the collision plane defined by the incident projectile (+z) and the transverse momentum of the recoil ion (+x).

5. Ionized electron spectra for 100, 300 and 500 keV/u $Ne^{10+}$ projected perpendicular (+y) to the collision plane defined by the incident projectile (+z) and the transverse momentum of the recoil ion (+x).

6. Ionized electron spectra for 100, 300 and 500 keV/u $Ne^{10+}$ in the collision plane defined by the incident projectile (+z) and the transverse momentum of the recoil ion (+x). The restrictions placed on the perpendicular component of the ejected electrons was $|p_y^d| \leq$ 0.05 a.u.

7. Ionized electron, projectile and recoil ion spectra for 100 keV/u $Ne^{10+}$. The collision plane is defined the same as in Fig. 6 with a coincidence of the recoil and projectile on the

emitted electron.

8. Ionized electron spectra for 100 keV/u $Ne^{10+}$ with the collision plane defined the same as in Fig. 6. The spectra were determined in coincidence with the transverse momentum of the recoil ion. For soft collisions, top figure, $|p_\perp^{rec}| \leq 0.5$ a.u., for intermediate collisions, 0.5 a.u. $\leq |p_\perp^{rec}| \leq 2.0$ a.u., and for violent collisions $|p_\perp^{rec}| \geq 2.0$ a.u.

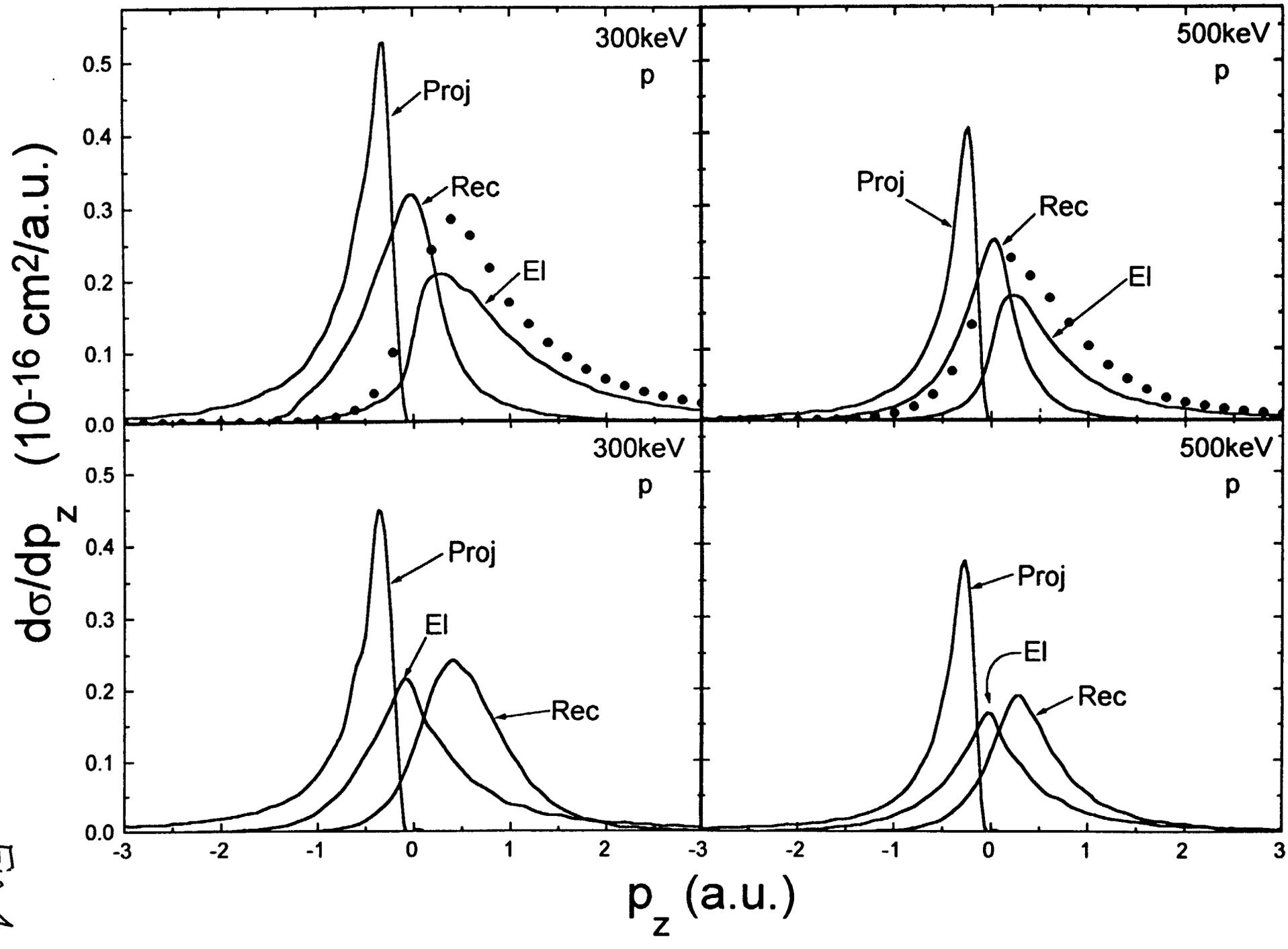
300keV
p
Proj
Rec
El
500keV
p
Proj
Rec
El
300keV
p
Proj
El
Rec
500keV
p
Proj
El
Rec
dσ/dp_z (10^-16 cm^2/a.u.)
p_z (a.u.)
0.0
0.1
0.2
0.3
0.4
0.5
-3
-2
-1
0
1
2
3

Fig. 4

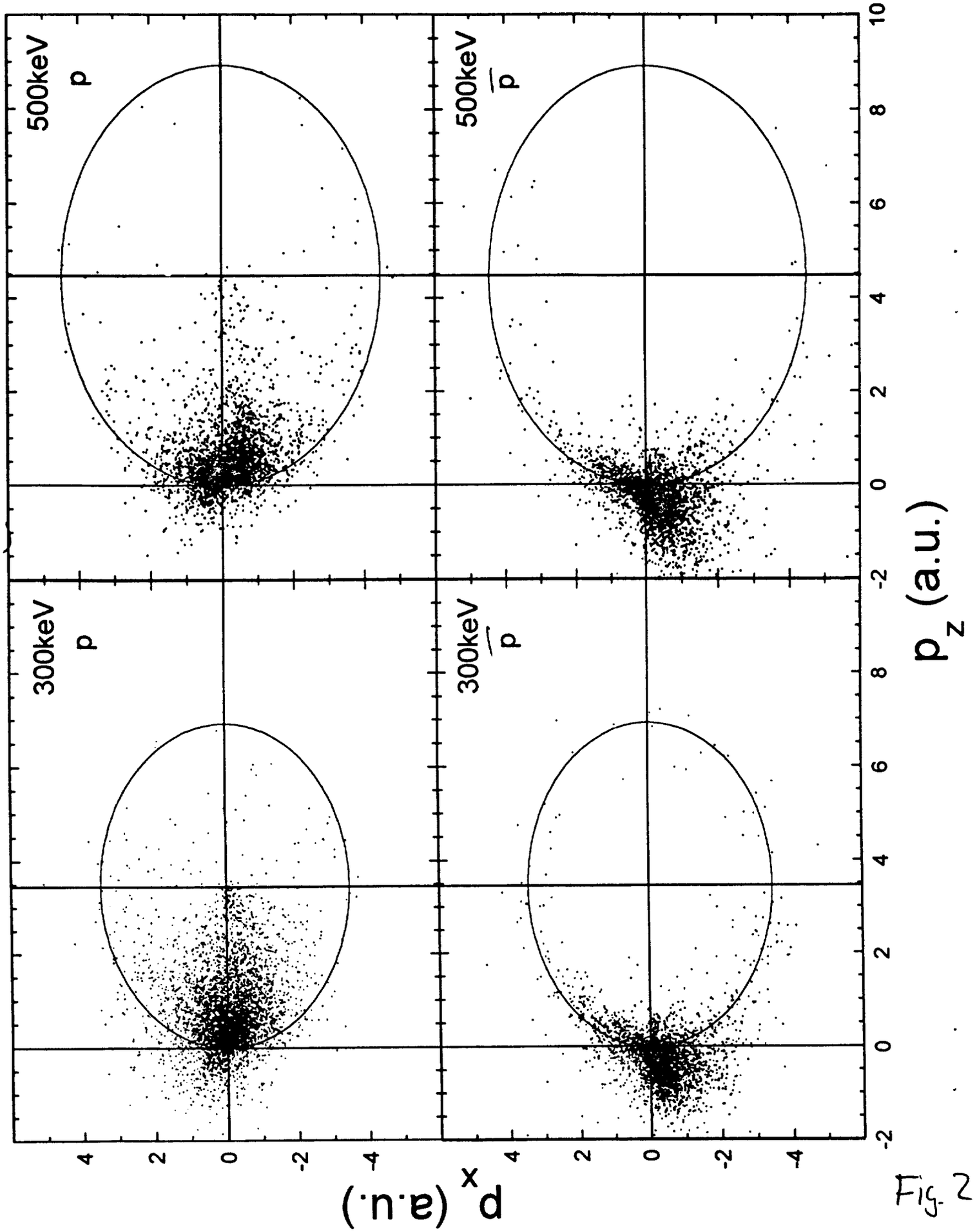


Fig. 2

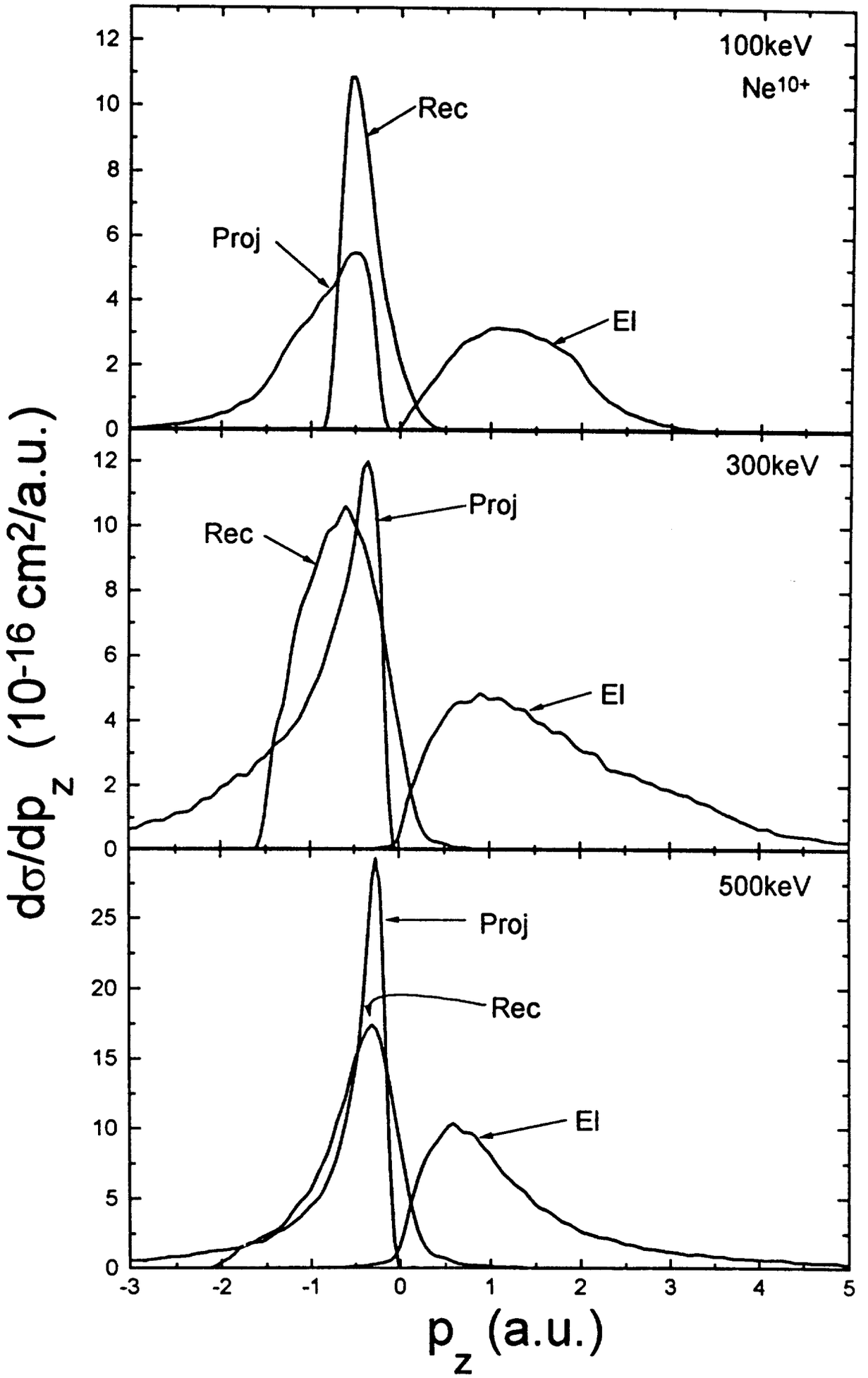
100keV
Ne10+
Rec
Proj
El
300keV
Proj
Rec
El
500keV
Proj
Rec
El
dσ/dpz (10-16 cm2/a.u.)
pz (a.u.)

Fig. 3

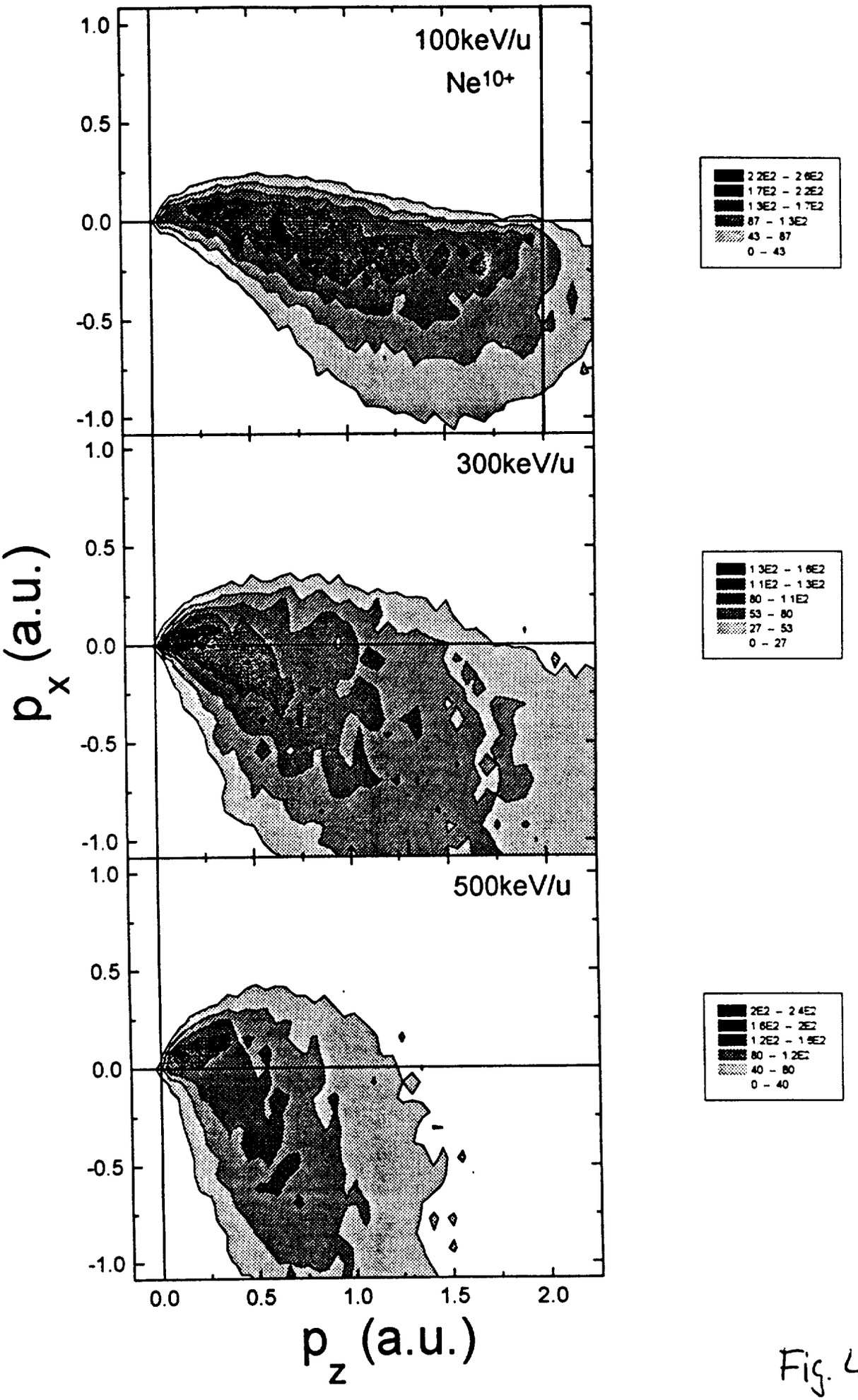
100keV/u
Ne10+
300keV/u
500keV/u
p_x (a.u.)
p_z (a.u.)
1.0
0.5
0.0
-0.5
-1.0
0.0
0.5
1.0
1.5
2.0
2.2E2 - 2.6E2
1.7E2 - 2.2E2
1.3E2 - 1.7E2
87 - 1.3E2
43 - 87
0 - 43
1.3E2 - 1.6E2
1.1E2 - 1.3E2
80 - 1.1E2
53 - 80
27 - 53
0 - 27
2E2 - 2.4E2
1.6E2 - 2E2
1.2E2 - 1.6E2
80 - 1.2E2
40 - 80
0 - 40

Fig. 4

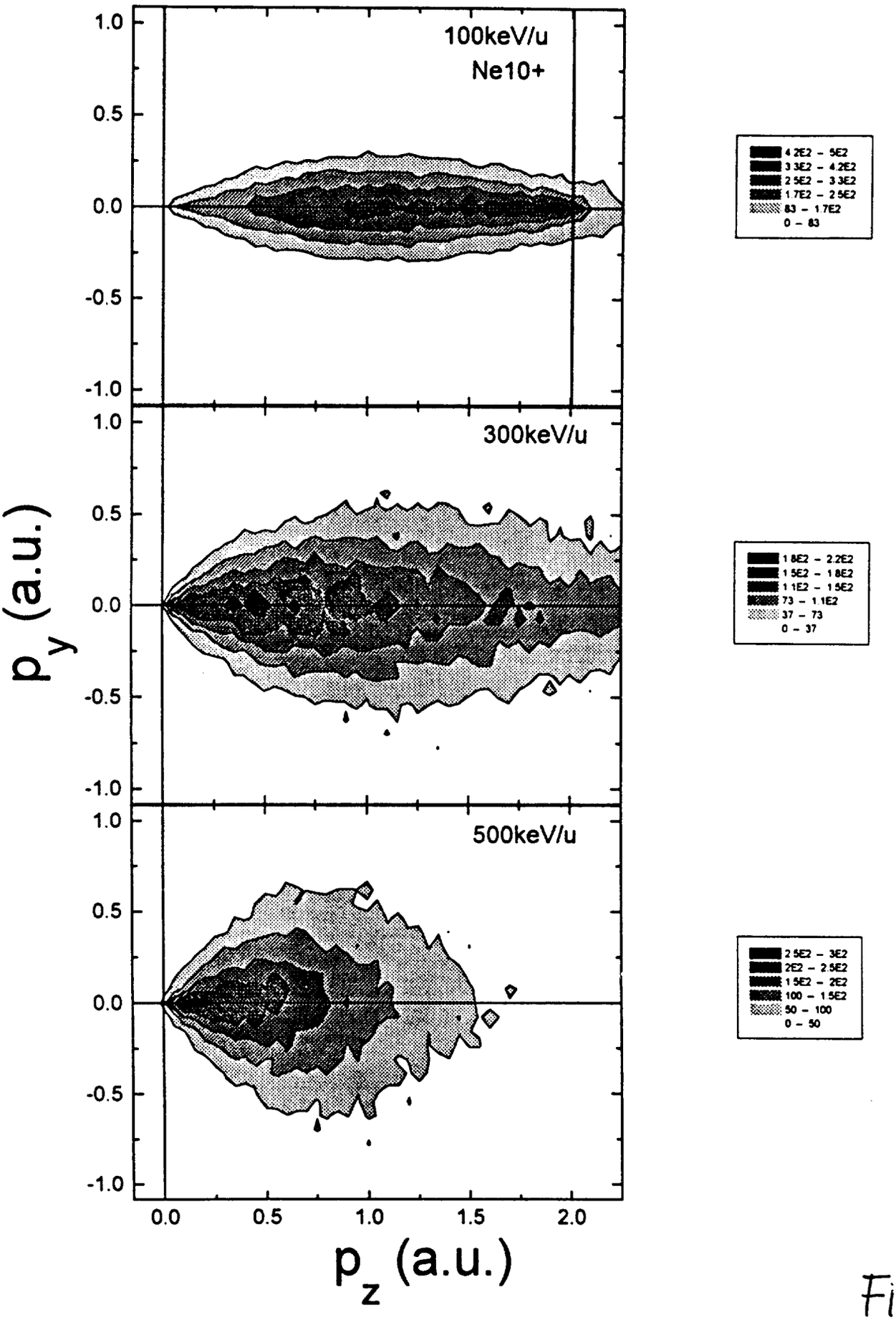
100keV/u
Ne10+
300keV/u
500keV/u
4.2E2 - 5E2
3.3E2 - 4.2E2
2.5E2 - 3.3E2
1.7E2 - 2.5E2
83 - 1.7E2
0 - 83
1.8E2 - 2.2E2
1.5E2 - 1.8E2
1.1E2 - 1.5E2
73 - 1.1E2
37 - 73
0 - 37
2.5E2 - 3E2
2E2 - 2.5E2
1.5E2 - 2E2
100 - 1.5E2
50 - 100
0 - 50
1.0
0.5
0.0
-0.5
-1.0
0.0
0.5
1.0
1.5
2.0
$p_y$ (a.u.)
$p_z$ (a.u.)

Fig. 5

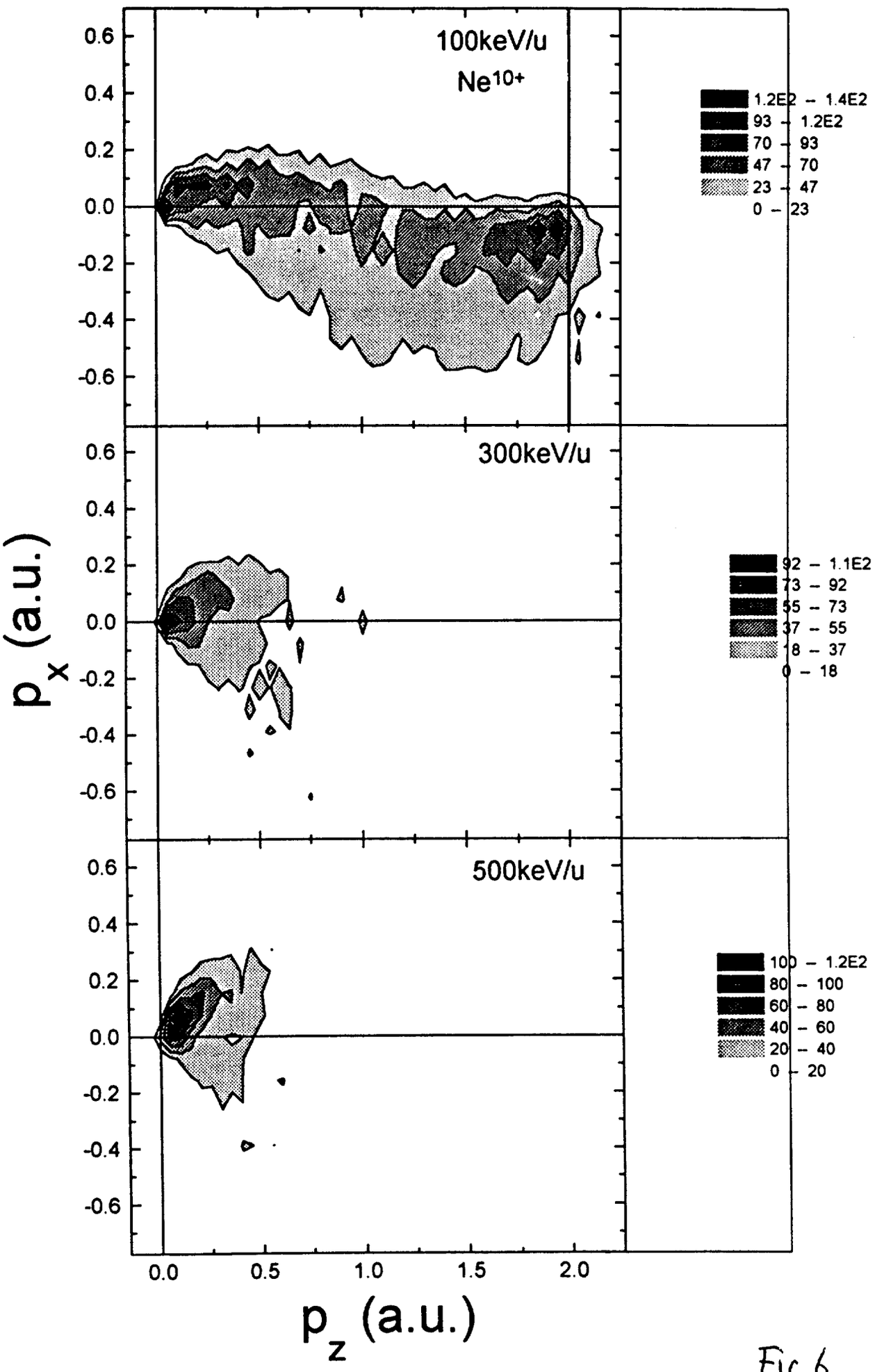
100keV/u
Ne10+
1.2E2 – 1.4E2
93 – 1.2E2
70 – 93
47 – 70
23 – 47
0 – 23
300keV/u
92 – 1.1E2
73 – 92
55 – 73
37 – 55
18 – 37
0 – 18
500keV/u
100 – 1.2E2
80 – 100
60 – 80
40 – 60
20 – 40
0 – 20
0.6
0.4
0.2
0.0
-0.2
-0.4
-0.6
0.0
0.5
1.0
1.5
2.0
p_x (a.u.)
p_z (a.u.)

Fig. 6

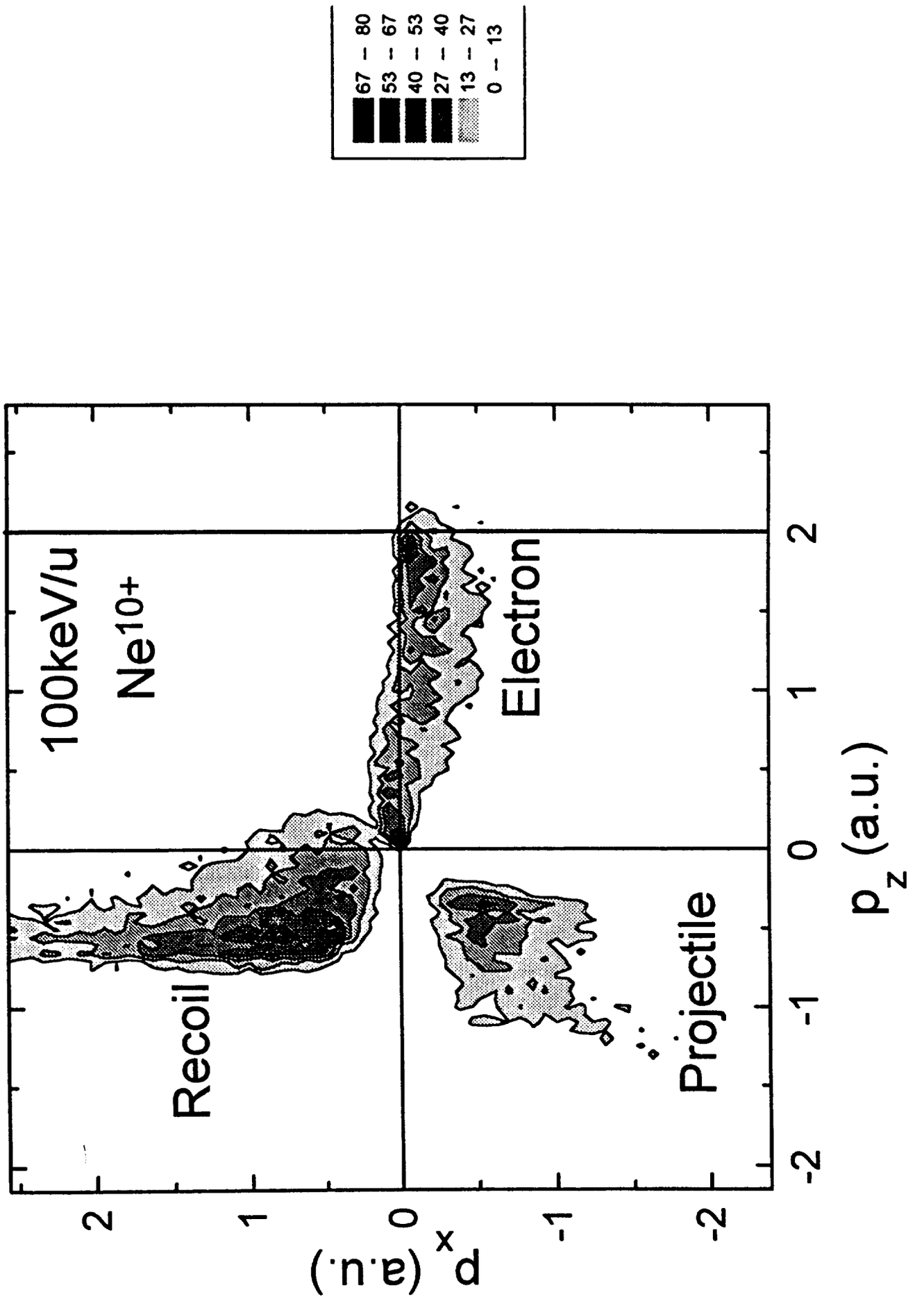
67 – 80
53 – 67
40 – 53
27 – 40
13 – 27
0 – 13
100keV/u
Ne10+
Electron
Recoil
Projectile
p_x (a.u.)
p_z (a.u.)
2
1
0
-1
-2

Fig. 7

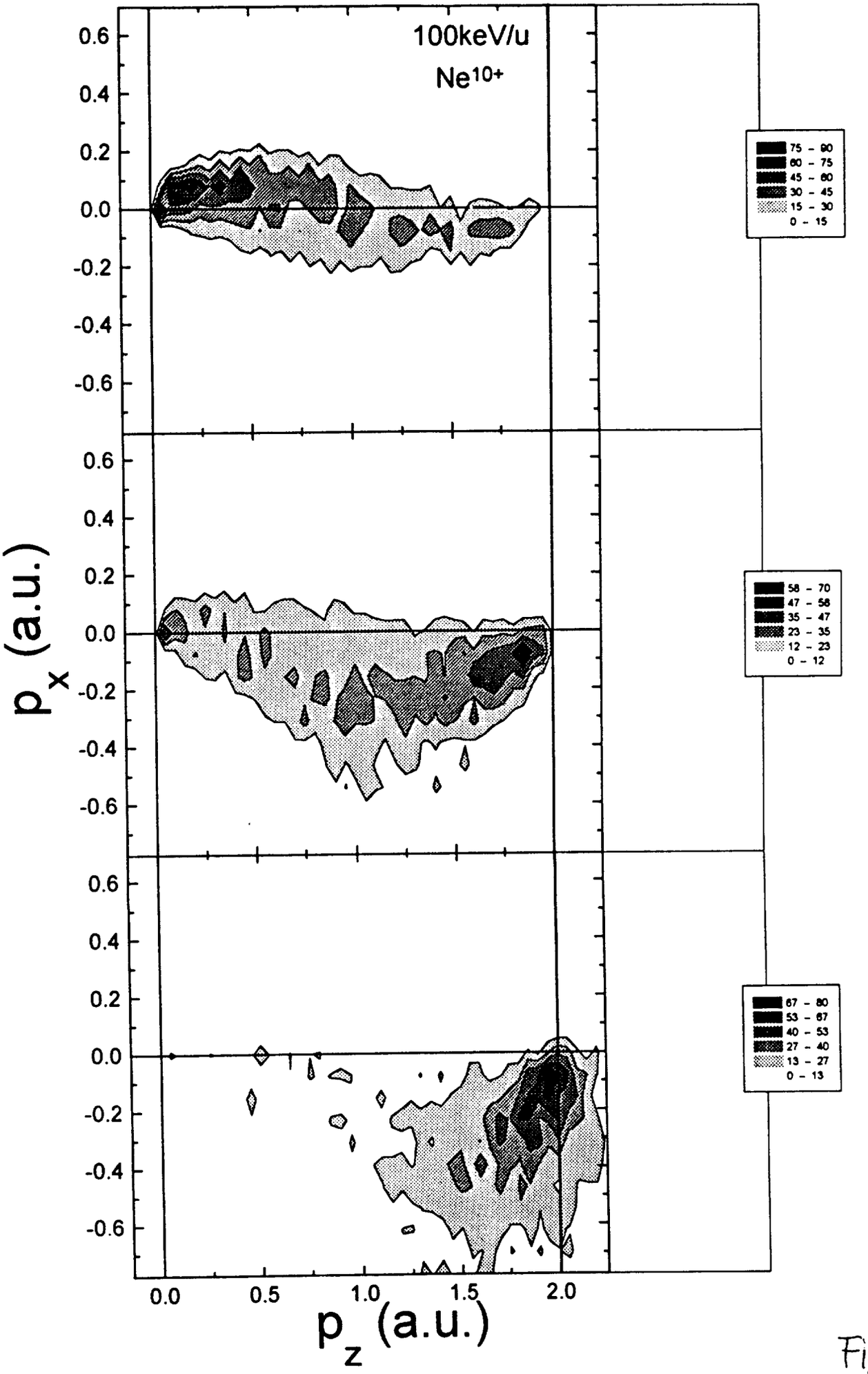
100keV/u
Ne10+
0.6
0.4
0.2
0.0
-0.2
-0.4
-0.6
75 - 90
60 - 75
45 - 60
30 - 45
15 - 30
0 - 15
58 - 70
47 - 58
35 - 47
23 - 35
12 - 23
0 - 12
67 - 80
53 - 67
40 - 53
27 - 40
13 - 27
0 - 13
p_x (a.u.)
0.0
0.5
1.0
1.5
2.0
p_z (a.u.)

Fig. 8